Journal of Fluids and Structures (2001) **15,** 867–884
doi:10.1006/jfls.2000.0381, available online at http://www.idealibrary.com on IDEAL®

AN INVERSE-DIRECT METHOD FOR PREDICTING THE VORTEX-INDUCED VIBRATIONS OF CYLINDERS IN UNIFORM AND NONUNIFORM FLOWS

R. A. Skop

Division of Applied Marine Physics, Rosenstiel School of Marine and Atmospheric Science University of Miami, Miami, FL 33149, U.S.A.

AND

G. Luo

Department of Mechanical & Industrial Engineering, University of Illinois, Urbana IL 61801, U.S.A.

(Received 13 July 2000, and in final form 19 February 2001)

An inverse-direct method for predicting the vortex-induced vibrations of uniform and nonuniform cylinders in uniform and nonuniform flows is developed. In this method, the fluid force acting per unit length on a uniform cylinder in a uniform flow is found by using known experimental results and inverting the equation of motion of the cylinder. This force is a function of the response parameter (structural damping divided by the ratio of displaced fluid mass to structural mass) and the frequency ratio (the ratio of the intrinsic shedding frequency to the structural natural frequency). The dependence of the fluid force on the frequency ratio is shown to explain the modal coupling patterns found for taut cables and beams in uniform flows. For nonuniform flows or nonuniform cylinders, the force is applied locally and varies along the cylinder, depending on the local values of the response parameter and frequency ratio. The predictions of the inverse-direct method for the vortex-induced vibrations of uniform and tapered pivoted cylinders in uniform and linearly sheared flows are compared with experimental data. The general agreement between the predictions and the data is quite good.

1. INTRODUCTION

Over the past several decades, numerous investigators have employed nonlinear oscillator equations of the van der Pol type to represent the fluctuating lift force produced on a cylinder by the vortex-shedding process (Hartlen & Currie 1970; Skop & Griffin 1973; Iwan & Blevins 1974; Skop & Griffin 1975; Iwan 1975). This representation for the lift force was based more on the similarity between the vortex-shedding process and the behavior of nonlinear oscillators than on the underlying fluid dynamics. The models, however, did succeed in identifying the response parameter as the controlling factor in determining the structural response (Skop & Griffin 1973; Iwan & Blevins 1974). The response parameter is defined, essentially, by the ratio of the structural damping to the ratio of the displaced fluid to structural masses. The models also succeeded in identifying the modal scaling principle for the structural response (Skop & Griffin 1975; Iwan 1975). The modal scaling principle collapses the responses of different-type structures to vortex shedding to a single curve through a mode shape factor. Many variations of the original

0889–9746/01/060867 + 18 $35.00/0

nonlinear oscillator models have since been proposed. Reviews can be found in Parkinson (1989) and Billah (1989).

More recently, efforts have been made to extend the nonlinear oscillator models to the prediction of vortex-induced vibrations of uniform and nonuniform cylinders in uniform and nonuniform flows (Bokaian 1994; Triantafyllou *et al.* 1994; Balasubramanian *et al.* 2000, 2001). For the most part, these efforts have generated predictions that are at considerable variance from experimental results. Balasubramanian *et al.* (2000) attribute this to the oversimplification of the underlying fluid dynamics that is implicit in nonlinear oscillator models.

In this paper, a new method for predicting the vortex-induced response of cylinders in uniform and nonuniform flows is developed. We term the method an inverse-direct method. In the inverse portion of the method, the equation of motion of a uniform cylinder in a uniform flow is inverted and known experimental results are used to determine the fluid force per unit length acting on the cylinder. Due to the scatter in the data, the calculated force is, in some sense, a best-fit approximation. The force depends on two variables: the response parameter and the frequency ratio (the ratio of the intrinsic shedding frequency to the structural natural frequency).

In the direct portion of the method, the calculated fluid force is applied locally along the cylinder. We show that the dependency of the force on the frequency ratio provides an explanation of the modal coupling patterns found experimentally for taut cables and beams in uniform flows. For nonuniform flows or nonuniform cylinders, the force varies along the cylinder depending on the local values of the response parameter and frequency ratio. The predictions of the inverse-direct method are compared with experimental data for uniform and tapered pivoted cylinders in uniform and sheared flows. The agreement between the predictions and the data are quite good, especially when account is taken of the scatter in the data for uniform cylinders in uniform flows. The predicted peak vibration amplitudes range from -11% to $+25\%$ of the measured ones. The predicted flow velocities at which the peak amplitudes occur are within -6% to $+20\%$ of the measured flow velocities. The main discrepancy between the predictions and the measured data is in the extent of the lock-in regions, the predicted extents tending to be somewhat wider than the measured ones.

2. UNIFORM CYLINDERS IN UNIFORM FLOWS

2.1. The Stall Term

We take ω_S as the naturally occurring vortex shedding frequency and ω_n as the natural frequency of a spring-mounted, uniform circular cylinder. The vortex-shedding frequency is given by

$$\omega_S = \frac{2\pi S V}{D}. \tag{1}$$

Here, S is the Strouhal number taken as $S = 0{\cdot}21$, V is the flow speed and D is the cylinder diameter. The structural response to the vortex-produced oscillating lift force is governed by (Skop & Balasubramanian 1997)

$$\frac{\mathrm{d}^2 y}{\mathrm{d}t^2} + 2\xi\omega_n \frac{\mathrm{d}y}{\mathrm{d}t} + \omega_n^2 y = \frac{\rho V^2}{2(m_s + m_a)}\left[Q - \frac{2\alpha}{\omega_S}\left(\frac{\omega_S}{\omega_n}\right)^k \frac{\mathrm{d}y}{\mathrm{d}t}\right]. \tag{2}$$

In this equation, t is time and y is the structural displacement referenced to the diameter D. The mass and added mass of the cylinder, both per unit length, are denoted respectively by

m_s and m_a. The corrected structural-damping ratio ξ is defined by

$$\xi = \xi_s \sqrt{\frac{m_s}{m_s + m_a}}, \tag{3}$$

where ξ_s is the actual structural damping ratio as measured in air. The excitation component of the fluctuating lift coefficient is denoted by Q. The second term in the brackets in equation (2) is the stall component of the fluctuating lift coefficient. In this term, the constant α, designated the stall parameter, and the exponent k, designated the stall coefficient, are independent quantities to be determined. The stall component provides that the magnitude of the fluctuating lift force has a negative slope for large structural motions. The inclusion of the stall component was first suggested by Triantafyllou *et al.* (1994) based on lift measurements on mechanically oscillated cylinders. Skop & Balasubramanian (1997) also included the stall component in a reexamination of nonlinear oscillator models. They demonstrated that its inclusion provided for a self-limiting structural response at zero structural damping. As will be shown, the same is true for the indirect–direct method developed herein. Both Triantafyllou *et al.* and Skop & Balasubramanian were concerned with near-resonant conditions, $\omega_S \approx \omega_n$, and the term $(\omega_S/\omega_n)^k$ in the stall component did not appear in their works. We show now that the term is necessary to provide the correct asymptotic behavior of equation (2) for large flow speeds.

Substituting for V in terms of ω_S from equation (1) and letting $t = \tau/\omega_n$ where τ is a dimensionless time, equation (2) becomes

$$\ddot{y} + 2\xi\dot{y} + y = \mu\Omega_S^2(\mathrm{Q} - 2\alpha\Omega_S^{k-1}\dot{y}). \tag{4}$$

Here, a dot denotes differentiation with respect to τ. The dimensionless frequency Ω_S is defined by $\Omega_S = \omega_S/\omega_n$ and the mass ratio parameter μ is given by

$$\mu = \frac{\rho D^2}{8\pi^2 S^2(m_s + m_a)}. \tag{5}$$

Far from resonance, experiments show that $Q = C_{L0}\sin\Omega_S\tau$, where C_{L0} is the oscillating lift coefficient over a stationary cylinder. Substituting for Q in equation (4) and rearranging terms, we obtain the equation for the cylinder displacement as

$$\ddot{y} + 2(\xi + \mu\alpha\Omega_S^{k+1})\dot{y} + y = \mu\Omega_S^2 C_{L0}\sin\Omega_S\tau. \tag{6}$$

The steady-state solution to this equation is $y = A\sin(\Omega_S\tau + \varphi)$, where (Thomson 1965)

$$A = \frac{\mu\Omega_S^2 C_{L0}}{\sqrt{(1 - \Omega_S^2)^2 + [2(\xi + \mu\alpha\Omega_S^{k+1})\Omega_S]^2}} \tag{7}$$

and

$$\tan\varphi = \frac{2(\xi + \mu\alpha\Omega_S^{k+1})\Omega_S}{\Omega_S^2 - 1} \tag{8}$$

Let us now consider the asymptotic behavior of y, $\dot{y}$ and $\ddot{y}$ for large Ω_S; that is, at large V. The asymptotic behavior is, in turn, given by the asymptotic behavior of A, $\Omega_S A$ and $\Omega_S^2 A$, respectively. From equation (7), we then find

$$y \propto \frac{1}{\Omega_S^k}, \qquad \dot{y} \propto \frac{1}{\Omega_S^{k-1}} \quad \text{and} \quad \ddot{y} \propto \frac{1}{\Omega_S^{k-2}}. \tag{9a, b, c}$$

TABLE 1
Asymptotic behavior of the cylinder response for large Ω_S

k	y	$\dot{y}$	$\ddot{y}$
0	Finite	Infinite	Infinite
1	Zero	Finite	Infinite
2	Zero	Zero	Finite
3	Zero	Zero	Zero

The asymptotic behavior of the cylinder response is summarized in Table 1 as a function of k. From Table 1, we see that, for $k = 0$, y and $\dot{y}$ do not go to zero as is observed experimentally. In fact, $\dot{y}$ becomes infinite for large Ω_S. We also observe from Table 1 that setting $k = 1$ does not resolve the problem since $\dot{y}$ remains finite. For the stall term to produce correct asymptotic results, we must have $k \geq 2$.

2.2. Lock-In

Let us return to equation (2) and write Q as $Q = C_L \sin \omega_f t$, where C_L is the oscillating lift coefficient and ω_f is some forcing frequency. Using the dimensionless time τ, equation (2) then becomes

$$\ddot{y} + 2(\xi + \mu\alpha\Omega_S^{k+1})\dot{y} + y = \mu\Omega_S^2 C_L \sin \Omega_f \tau, \tag{10}$$

where $\Omega_f = \omega_f/\omega_n$. One of the fundamental features of vortex-induced vibrations is resonant lock-in (Sarpkaya & Isaacson 1981). As the vortex-shedding frequency approaches the structural natural frequency, the intrinsic vortex-shedding frequency becomes suppressed. The frequencies of vortex shedding and structural oscillation collapse into a single frequency close to the structural natural frequency, over a range of flow velocities, and the structure undergoes resonant vibrations. We define Ω_{S1} as the intrinsic Strouhal shedding frequency at the beginning of the lock-in range and Ω_{S2} as the intrinsic Strouhal shedding frequency at the end of the lock-in range. The behavior of the frequency Ω_f for all flow velocities is then closely approximated by

$$\Omega_f = \begin{cases} \Omega_S & \text{if } \Omega_S < \Omega_{S1} \text{ or } \Omega_S > \Omega_{S2}, \\ 1 & \text{if } \Omega_{S1} \leq \Omega_S \leq \Omega_{S2}. \end{cases} \tag{11}$$

We note here that Khalak & Williamson (1999) and Gharib (1999) have reported deviations from classical lock-in for vortex-induced vibrations at small values of $1/\mu$. They find instead that $\Omega_f = \Omega_f(\Omega_S, 1/\mu)$ if $\Omega_{S1} \leq \Omega_S \leq \Omega_{S2}$ where, additionally, $\Omega_f(\Omega_S, 1/\mu) \leq \Omega_S$. Their findings can be incorporated into equation (11) if necessary. For most practical applications, however, $1/\mu$ is large enough so that equation (11) is valid.

2.3. Modal Scaling

Equation (2) can be extended to a uniform elastic cylinder responding purely in its ith mode to vortex forcing in a uniform flow. Following the modal-scaling principle (Skop & Griffin 1975; Iwan 1975), we have for this situation that the structural displacement $y(x, t)$ referenced to the diameter D is given by

$$y = \Gamma_i^{1/2} r_i(t) \psi_i(x). \tag{12}$$

Here, x is the measure of distance along the cylinder of total length L and $\psi_i(x)$ is ith normal mode of response of the cylinder. The modal response factor for the ith mode is denoted by $r_i(t)$ and the modal scaling factor Γ_i is defined by

$$\Gamma_i = \int_0^L \psi_i^2(x)\,\mathrm{d}x \Big/ \int_0^L \psi_i^4(x)\,\mathrm{d}x. \tag{13}$$

Similarly, the lift force $Q(x, t)$ is written as

$$Q = \Gamma_i^{1/2} q_i(t)\psi_i(x), \tag{14}$$

where $q_i(t)$ is the modal lift factor for the ith mode. Substituting equations (12) and (14) into (2), then gives the equation of motion for the response of the ith mode in a uniform flow as

$$\frac{\mathrm{d}^2 r_i}{\mathrm{d}t^2} + 2\xi_i\omega_{n,i}\frac{\mathrm{d}r_i}{\mathrm{d}t} + \omega_{n,i}^2 r_i = \frac{\rho V^2}{2(m_s + m_a)}\left[q_i - \frac{2\alpha}{\omega_S}\left(\frac{\omega_S}{\omega_{n,i}}\right)^k \frac{\mathrm{d}r_i}{\mathrm{d}t}\right]. \tag{15}$$

In this equation, $\omega_{n,i}$ is the natural frequency of the ith normal mode and the damping ξ_i is defined by

$$\xi_i = \xi_{s,i}\sqrt{\frac{m_s}{m_s + m_a}}, \tag{16}$$

where $\xi_{s,i}$ is the actual structural damping ratio of the ith mode as measured in air.

Substituting for V in terms of ω_S from equation (1) and letting $t = \tau_i/\omega_{n,i}$ where τ_i is a dimensionless time for the ith mode, equation (15) becomes

$$\ddot{r}_i + 2(\xi_i + \mu\alpha\Omega_{S,i}^{k+1})\dot{r}_i + r_i = \mu\Omega_{S,i}^2 C_{L,i}\sin\Omega_{f,i}\tau_i. \tag{17}$$

Here, a dot denotes differentiation with respect to τ_i and the dimensionless frequency $\Omega_{S,i}$ is defined by $\Omega_{S,i} = \omega_S/\omega_{n,i}$. In arriving at equation (17), we have expressed $q_i(t)$ as $q_i = C_{L,i}\sin\omega_f t$, where $C_{L,i}$ is the oscillating modal lift coefficient for the ith mode and where ω_f is again some forcing frequency. The dimensionless forcing frequency $\Omega_{f,i}$ is defined by $\Omega_{f,i} = \omega_f/\omega_{n,i}$.

2.4. The Fluid Force

Resonant lock-in is also a characteristic feature of the vortex-induced vibrations of an elastic cylinder responding purely in its ith mode to vortex forcing. Hence, we have that the behavior of the forcing frequency $\Omega_{f,i}$ is closely approximated by

$$\Omega_{f,i} = \begin{cases} \Omega_{S,i} & \text{if } \Omega_{S,i} < \Omega_{S1} \text{ or } \Omega_{Si} > \Omega_{S2}, \\ 1 & \text{if } \Omega_{S1} \le \Omega_{S,i} \le \Omega_{S2}. \end{cases} \tag{18}$$

We further define the oscillating modal lift coefficient $C_{L,i}$ for the ith mode as

$$C_{L,i} = \begin{cases} 0 & \text{if } \Omega_{S,i} < \Omega_{S1} \text{ or } \Omega_{Si} > \Omega_{S2}, \\ C_{L,i}(\Omega_{S,i}) & \text{if } \Omega_{S1} \le \Omega_{S,i} \le \Omega_{S2}. \end{cases} \tag{19}$$

(Note that, strictly, we should have $C_{L,i} = C_{L0}$ if $\Omega_{S,i} < \Omega_{S1}$ or $\Omega_{Si} > \Omega_{S2}$. However, the structural response is insignificant outside of the resonant lock-in region, so we lose little by taking $C_{L,i} = 0$ there.)

With equations (18) and (19), the solution to equation (17) for the modal response factor r_i is found as

$$r_i = \begin{cases} 0 & \text{if } \Omega_{S,i} < \Omega_{S1} \text{ or } \Omega_{S,i} > \Omega_{S2}, \\ -A_i \cos \tau_i & \text{if } \Omega_{S1} \le \Omega_{S,i} \le \Omega_{S2}. \end{cases} \tag{20}$$

where the modal response amplitude A_i is given by

$$A_i = \frac{\Omega_{S,i}^2 C_{L,i}}{2(S_{G,i} + \alpha \Omega_{S,i}^{k+1})}. \tag{21}$$

In writing equation (21), we have introduced the modal response parameter $S_{G,i}$ defined by

$$S_{G,i} = \frac{\xi_i}{\mu}. \tag{22}$$

Inverting equation (21), $C_{L,i}$ is obtained as

$$C_{L,i} = \frac{2(S_{G,i} + \alpha \Omega_{S,i}^{k+1}) A_i}{\Omega_{S,i}^2}. \tag{23}$$

Hence, $C_{L,i}$ can be determined if the behavior of A_i through the resonant lock-in region is known.

Bokaian (1994) has examined a large number of vortex-induced vibration experiments for uniform cylinders in uniform flows. Though there is substantial scatter in the data due to differences in facilities, aspect ratios, end conditions, etc., he finds that the behavior of A_i is similar for each experiment. Specifically, he finds that A_i can be approximated by

$$A_i = A_{\max,i} H(V_{r,i}). \tag{24}$$

Here, $A_{\max,i}$ is the maximum value reached by A_i and $H(V_{r,i})$ is a universal shape function dependent only on the reduced velocity $V_{r,i}$. The reduced velocity is defined by

$$V_{r,i} = \frac{V}{f_{n,i} D} = \frac{\Omega_{S,i}}{S}, \tag{25}$$

where the frequency $f_{n,i}$ is related to the radial frequency $\omega_{n,i}$ through $f_{n,i} = \omega_{n,i}/(2\pi)$. Bokaian gives the shape function as

$$H = (V_{r,i} - V_{r1})(V_{r,i} - V_{r2})(\gamma V_{r,i} + \lambda). \tag{26}$$

Here, $V_{r1} = \Omega_{S1}/S$ and $V_{r2} = \Omega_{S2}/S$ are the reduced velocities at the beginning and end of the lock-in region, respectively. The coefficients γ and λ are defined by

$$\gamma = \frac{V_{r1} + V_{r2} - 2V_{rp}}{(V_{r1} - V_{rp})^2 (V_{r2} - V_{rp})^2} \tag{27}$$

and

$$\lambda = \frac{V_{r1} V_{r2} - 2(V_{r1} + V_{r2}) V_{rp} + 3V_{rp}^2}{(V_{r1} - V_{rp})^2 (V_{r2} - V_{rp})^2}. \tag{28}$$

In these definitions, V_{rp} is the reduced velocity at which $A_{\max,i}$ occurs. Although Bokaian did not mention it, the constraint $3V_{rp} - 2V_{r1} - V_{r2} \ge 0$ must be satisfied for $H(V_{r,i})$ to remain positive throughout V_{r1} to V_{r2}.

Sarpkaya & Isaacson (1981) have discussed the values of V_{r1}, V_{r2} and V_{rp}. Again, there is substantial scatter in the data. For air, we use $V_{r1} = 5$, $V_{r2} = 8$ and $V_{rp} = 6$. For water, we

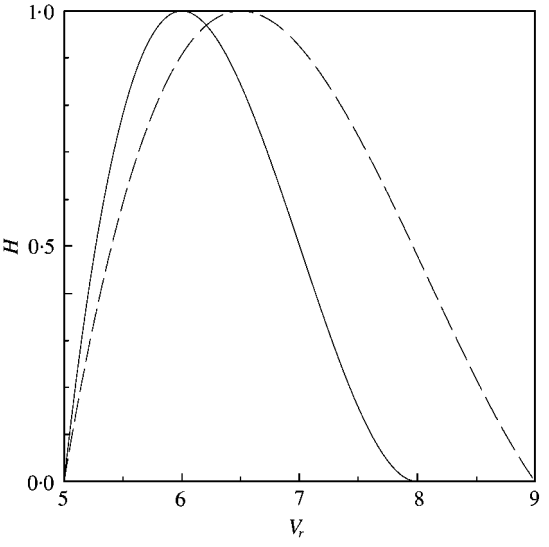

Figure 1. The universal shape function $H(V_r)$ for vortex-excited vibrations. —, for air; – – for water.

select $V_{r1} = 5$, $V_{r2} = 9$ and $V_{rp} = 6{\cdot}5$. The universal shape function $H(V_{r,i})$ is plotted in Figure 1 for both air and water. We note that Khalak & Williamson (1999) have reported deviations from V_{r1} and V_{r2} for vortex-induced vibrations at small values of $1/\mu$. They find that these lower and upper lock-in bounds are functions of $1/\mu$. These findings can be incorporated in the selection of V_{r1} and V_{r2} if necessary.

To complete the determination of $C_{L,i}$, the maximum value $A_{\max,i}$ of the modal response amplitude must be specified. It has become well established that, within experimental scatter, $A_{\max,i}$ depends only on the value of the modal response parameter $S_{G,i}$; that is $A_{\max,i} = A_{\max}(S_{G,i})$ (Skop & Griffin 1973; Iwan & Blevins 1974; Sarpkaya & Isaacson 1981; Khalak & Williamson 1999). The existing data points for $A_{\max}$ are plotted versus S_G in Figure 2. A least-squares fit to the natural logarithm of the data points, given by

$$A_{\max} = \exp(-0{\cdot}938 S_G), \tag{29}$$

is also plotted in the figure. Combining equations (19), (23) and (24), we obtain the oscillating modal lift coefficient $C_{L,i}$ for the ith mode as

$$C_{L,i} = \begin{cases} 0 & \text{if } V_{r,i} < V_{r1} \text{ or } V_{r,i} > V_{r2}, \\ \dfrac{2(S_{G,i} + \alpha\Omega_{S,i}^{k+1}) A_{\max}(S_{G,i}) H(V_{r,i})}{\Omega_{S,i}^2} & \text{if } V_{r1} \le V_{r,i} \le V_{r2}. \end{cases} \tag{30}$$

Here $A_{\max}(S_{G,i})$ is defined by equation (29), $H(V_{r,i})$ by equation (26), and the relation between $\Omega_{S,i}$ and $V_{r,i}$ by equation (25).

3. MODAL EQUATIONS OF MOTION

The structural response of an elastic cylinder to vortex-produced oscillating lift forces is governed by

$$\frac{\partial^2 y}{\partial t^2} + \frac{c}{m_s + m_a}\frac{\partial y}{\partial t} + \frac{\text{stiffness}}{m_s + m_a} y = \mu\omega_S^2 \frac{D}{D_{\text{ref}}}\left[Q - \frac{2\alpha}{\omega_S}\left(\frac{\omega_S}{\omega_n}\right)^k \frac{\partial y}{\partial t}\right], \tag{31}$$

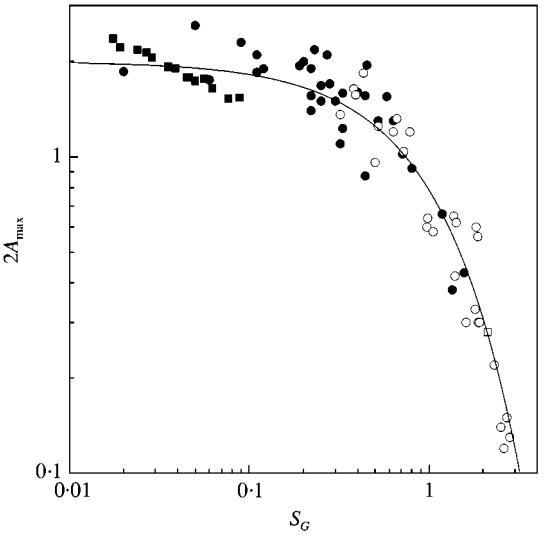

Figure 2. Experimental measurements of the modally normalized, maximum structural response amplitude A_{max} versus the response parameter S_G. The open symbols are in-air measurements, the closed symbols are in-water measurements. ○ and ●, from the appendix in Skop & Balasubramanian (1997); □, from Balasubramanian *et al.* (2000); ■, from Khalak & Williamson (1999); —, least-squares fit to the data, given by equation (29).

where c is the structural damping per unit length and "stiffness" represents the elastic properties of the system. Also, D_{ref} denotes the diameter by which the cylinder displacement is nondimensionalized. We now expand $y(x, t)$ as

$$y = \sum_i \Gamma_i^{1/2} r_i(t)\psi_i(x), \tag{32}$$

and, following the modal scaling principle, $Q(x, t)$ as

$$Q = \sum_i \Gamma_i^{1/2} q_i(t)\psi_i(x) = \sum_i \Gamma_i^{1/2} C_{L,i}\psi_i(x)\sin\omega_{f,i}t. \tag{33}$$

Here, as previously, $\omega_{f,i}/\omega_{n,i} = 1$ if $\Omega_{S1} \leq (\omega_S/\omega_{n,i}) \leq \Omega_{S2}$ and $C_{L,i}$ is defined by equation (30). Since $C_{L,i} = 0$ if $(\omega_S/\omega_{n,i}) < \Omega_{S1}$ or $(\omega_S/\omega_{n,i}) > \Omega_{S2}$, equation (33) can be recast as

$$Q = \sum_i \Gamma_i^{1/2} C_{L,i}\psi_i(x)\sin\omega_{n,i}t. \tag{34}$$

Applying equations (32) and (34), (31) becomes

$$\sum_i \Gamma_i^{1/2}\left(\frac{\mathrm{d}^2 r_i}{\mathrm{d}t^2} + 2\xi_i\omega_{n,i}\frac{\mathrm{d}r_i}{\mathrm{d}t} + \omega_{n,i}^2 r_i\right)\psi_i$$
$$= \mu\omega_S^2\frac{D}{D_{ref}}\sum_i \Gamma_i^{1/2}\left\{C_{L,i}\sin\omega_{n,i}t - \frac{2\alpha}{\omega_S}\left(\frac{\omega_S}{\omega_{n,i}}\right)^k\frac{\mathrm{d}r_i}{\mathrm{d}t}\right\}\psi_i. \tag{35}$$

In general, μ, ω_S, D and $C_{L,i}$ can be functions of the distance x along the cylinder because of nonuniformity of the cylinder or nonuniformity of the flow. Multiplying equation (35) by ψ_j, integrating over the length L of the cylinder, and employing the orthogonality condition,

$$\int_0^L \psi_i\psi_j\,\mathrm{d}x = M_j\delta_{ij}, \tag{36}$$

where the orthogonal weight M_j is determined from the integration and where δ_{ij} is the Kronecker delta, equation (35) is converted into

$$\frac{\mathrm{d}^2 r_j}{\mathrm{d}t^2} + 2\xi_j \omega_{n,i} \frac{\mathrm{d}r_j}{\mathrm{d}t} + \omega_{n,j}^2 r_j$$
$$= \frac{1}{M_j \Gamma_j^{1/2}} \sum_i \Gamma_i^{1/2} \int_0^L \mu \omega_S^2 \frac{D}{D_{\mathrm{ref}}} \left\{ C_{L,i} \sin \omega_{n,i} t - \frac{2\alpha}{\omega_S} \left(\frac{\omega_S}{\omega_{n,i}} \right)^k \frac{\mathrm{d}r_i}{\mathrm{d}t} \right\} \psi_i \psi_j \, \mathrm{d}x. \tag{37}$$

Equation (37) determines the reaction of the modal response factors r_j to vortex-produced oscillating lift forces.

4. TAUT CABLES, BEAMS AND MODAL PARTICIPATION

Let us now consider uniform taut cables and uniform beams in uniform flows. For this situation, equation (37) for the modal response factor r_j (or r_i) becomes

$$\frac{\mathrm{d}^2 r_i}{\mathrm{d}t^2} + 2\left[\xi_i \omega_{n,i} + \mu\alpha\omega_S \left(\frac{\omega_S}{\omega_{n,i}} \right)^k \right] \frac{\mathrm{d}r_i}{\mathrm{d}t} + \omega_{n,i}^2 r_i = \mu \omega_S^2 C_{L,i} \sin \omega_{n,i} t. \tag{38}$$

Substituting for $C_{L,i}$ from equation (30), the solution for r_i reduces, by design, to

$$r_i = \begin{cases} 0 & \text{if } V_{r,i} < V_{r1} \text{ or } V_{r,i} > V_{r2}, \\ -A_{\max}(S_{G,i}) H(V_{r,i}) \cos \omega_{n,i} t & \text{if } V_{r1} \le V_{r,i} \le V_{r2}. \end{cases} \tag{39}$$

Hence, we have that the ith mode participates in the overall response, given by the summation in equation (32), if $V_{r1} \le V_{r,i} \le V_{r2}$.

For a taut cable, the ith natural frequency $f_{n,i}$ can be expressed in terms of the fundamental natural frequency $f_{n,1}$ through the relation $f_{n,i} = i f_{n,1}$. Using equation (25) for $V_{r,i}$, the criterion for the participation of the ith mode in the overall cable response becomes

$$i V_{r1} \le V_{r,1} \le i V_{r2}. \tag{40}$$

The modal participation diagram for a taut cable in water ($V_{r1} = 5$, $V_{r2} = 9$) is shown in Figure 3. In this figure, the horizontal error bars mark the extent over $V_{r,1}$ for which the ith mode is excited. For $5 \le V_{r,1} \le 9$, only the first mode is excited. For $10 \le V_{r,1} \le 15$, only the second mode is excited, while, for $15 \le V_{r,1} \le 18$, both the second and third modes participate in the cable response. For $18 \le V_{r,1} \le 20$, only the third mode is excited, while the fourth mode joins in for $V_{r,1} \ge 20$, and so on. This modal participation behavior is very similar to that found by Griffin *et al.* (1980) in tow tank tests of marine cables.

For a beam, the ith natural frequency $f_{n,i}$ can be expressed in terms of the fundamental natural frequency $f_{n,1}$ through the relation $f_{n,i} = \beta_i f_{n,1}$ where the factor β_i depends on the beam boundary conditions. The values of β_i for various beam boundary conditions can be found in Thomson (1965). Using equation (25) for $V_{r,i}$, the criterion for the participation of the ith mode in the overall beam response becomes

$$\beta_i V_{r1} \le V_{r,1} \le \beta_i V_{r2}. \tag{41}$$

The modal participation diagrams for a clamped–clamped beam and a clamped–free beam, both in water, are shown in Figures 4(a) and (b), respectively. We note that for a clamped–free beam the second mode does not begin to participate until $V_{r,1} > 31{\cdot}33$. This high value of $V_{r,1}$ explains why second mode vibrations have never been observed in cantilevered beam experiments, at least to the knowledge of the authors.

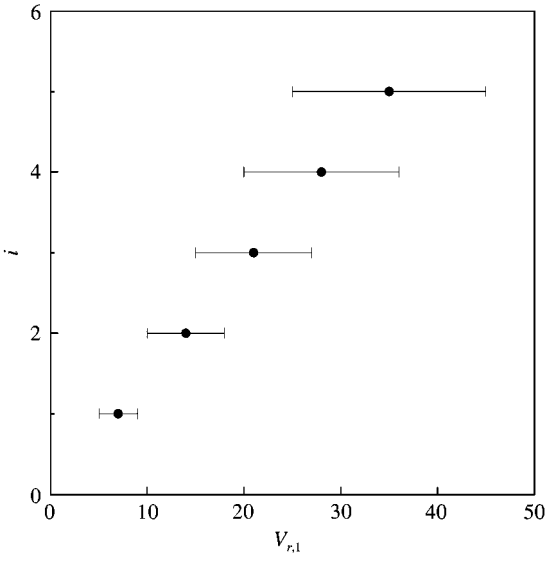

Figure 3. Modal participation diagram for a taut cable in water.

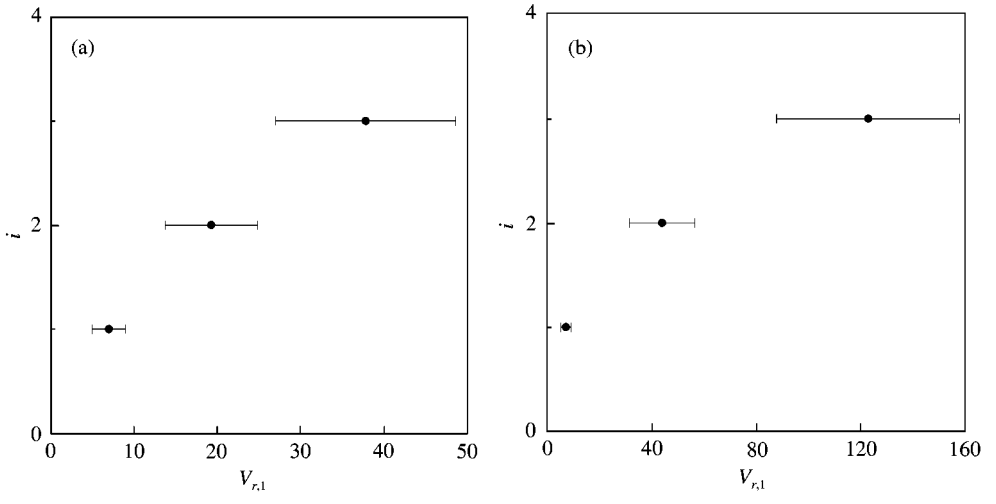

Figure 4. Modal participation diagrams for beams in water. (a) Clamped–clamped boundary conditions; (b) clamped–free boundary conditions.

5. PIVOTED CYLINDERS

We now turn our attention to pivoted cylinders. For a pivoted, rigid cylinder, the only nonzero mode of vibration is $\psi_1 = x/L$. From equation (13), we have $\Gamma_2^{1/2} = (5/3)^{1/2} = 1{\cdot}291$ and, from equation (36), $M_1 = L/3$. Dropping the extraneous subscripts for ease of notation and introducing $t = \tau/\omega_n$ and $x = Lz$ where z is a dimensionless distance, the cylinder response is obtained from equation (32) as

$$y(z, \tau) = 1{\cdot}291 z r(\tau). \tag{42}$$

The equation satisfied by the modal response factor r is found from equation (37) as

$$\ddot{r} + 2\left[\xi + 3\alpha \int_0^1 \frac{D}{D_{\text{ref}}}\, \mu \Omega_S^{k+1} z^2 \, \mathrm{d}z\right]\dot{r} + r = \left[3 \int_0^1 \frac{D}{D_{\text{ref}}} \mu \Omega_S^2 C_L z^2 \, \mathrm{d}z\right] \sin \tau. \tag{43}$$

Let us denote by $\Omega_{S,\min}$ and $\Omega_{S,\max}$ the minimum and maximum naturally occurring shedding frequencies along the cylinder. Then, if $\Omega_{S,\max} < \Omega_{S1}$ or if $\Omega_{S,\min} > \Omega_{S2}$, we have from equation (30) that $C_L = 0$ and, from equation (43), that $r = 0$. Otherwise, there is a region of shedding along the cylinder where $\Omega_{S1} \leq \Omega_S \leq \Omega_{S3}$. We then find $r = -A \cos \tau$, where

$$A = \frac{(3/D_{\text{ref}}) \int_0^1 D \mu \Omega_S^2 C_L z^2 \, \mathrm{d}z}{2[\xi + (3\alpha/D_{\text{ref}}) \int_0^1 D \mu \Omega_S^{k+1} z^2 \, \mathrm{d}z]}. \tag{44}$$

Substituting for C_L from equation (30), the expression for A can be rewritten as

$$A = \frac{\xi q_1 + \alpha q_2}{\xi + \alpha \Phi}, \tag{45}$$

where q_1, q_2 and Φ are defined by

$$q_1 = \frac{3}{D_{\text{ref}}} \int_0^1 A_{\max}(S_G) H(V_r) D z^2 \, \mathrm{d}z, \tag{46}$$

$$q_2 = \frac{3}{D_{\text{ref}}} \int_0^1 A_{\max}(S_G) H(V_r) D \mu \Omega_S^{k+1} z^2 \, \mathrm{d}z, \tag{47}$$

and

$$\Phi = \frac{3}{D_{\text{ref}}} \int_0^1 D \mu \Omega_S^{k+1} z^2 \, \mathrm{d}z. \tag{48}$$

Balasubramanian *et al.* (2000, 2001) have conducted wind tunnel experiments on the vortex-induced vibrations of uniform and tapered, pivoted cylinders in uniform and sheared flows. The uniform cylinder results are reported in Balasubramanian *et al.* (2000) and the tapered cylinder results are reported in Balasubramanian *et al.* (2001). The dimensions of the two cylinders used in the experiments are given in Figure 5. The cylinders were constructed from wood having a density of 540 kg/m^3. The tapered cylinder could be pivoted at either end. Two linearly sheared flows could be generated in the wind tunnel. One of these flows increased along the length of the cylinder and was given, in meters per second (m/s), by

$$V = V_0(1 + 0{\cdot}88Lz), \tag{49}$$

where V_0 denotes the value of the flow velocity at $z = 0$. The second flow decreased along the length of the cylinder and was given, also in m/s, by

$$V = V_0(1 - 0{\cdot}54Lz). \tag{50}$$

Balasubramanian *et al.* present their results as plots of the peak-to-peak tip displacement of the cylinder $2y_{\text{tip}}$ versus the reference reduced velocity $V_{r,\text{ref}} = V_{0{\cdot}5}/(f_n D_{\text{ref}})$, where $V_{0{\cdot}5} = V(z = 0{\cdot}5)$. The tip displacement is the amplitude of the cylinder motion at $z = 1$ and, from equations (42) and (45), is determined as

$$y_{\text{tip}} = 1{\cdot}291 \frac{\xi q_1 + \alpha q_2}{\xi + \alpha \Phi}. \tag{51}$$

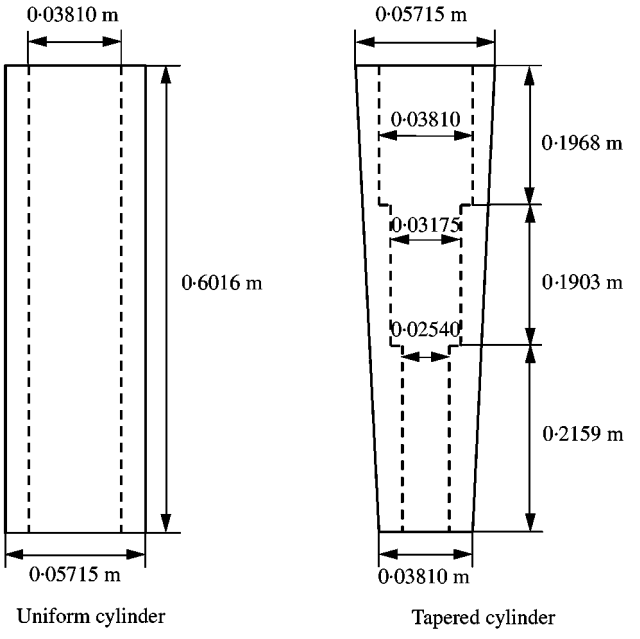

Figure 5. Schematics of the two cylinders used in the vortex-excited vibration experiments of Balasubramanian *et al.* (2000, 2001).

For our calculations, the value of k is taken as $k = 2$, the minimum allowable value. We will demonstrate shortly that the value selected for k has little influence on the results. The integrals in equations (46), (47) and (48) are evaluated using a 100-point trapezoidal integration. Since the experiments were performed in air, we also have $V_{r1} = 5$, $V_{r2} = 8$ and $V_{rp} = 6$.

5.1. Uniform Cylinder

The uniform cylinder had a length $L = 0{\cdot}6016$ m, a diameter $D = D_{\text{ref}} = 0{\cdot}05715$ m, a natural frequency $f_n = 20$ Hz and a damping ratio $\xi = 0{\cdot}0031$. The predicted and measured responses for the uniform flow case are shown in Figure 6. For this situation, the predicted response is the same for all values of the stall parameter α. From this figure, we note that the predicted and measured maximum values of $2y_{\text{tip}}$ are virtually identical. The predicted location of the maximum value is at $V_{r,\text{ref}} = 6$, which is 11% higher than the measured location of $V_{r,\text{ref}} \approx 5{\cdot}4$. This 11% difference is well within the scatter in the data from which V_{rp} was selected. The principle variance between the predicted and measured responses is in the extent of the lock-in region. The predicted lock-in region ranges from $V_{r,\text{ref}} = 5$ to 8 while the measured lock-in region ranges from $V_{r,\text{ref}} = 4{\cdot}7$ to $5{\cdot}6$. The measured lock-in region is somewhat narrower than is usually observed (Sarpkaya and Isaacson 1981).

The predicted and measured responses of the uniform cylinder for the linearly sheared flow cases are shown in Figure 7. The predicted response is shown for values of the stall parameter $\alpha = 0$, 1 and 1000. We note that, at least for the cases represented in Figure 7, the predicted response is relatively insensitive to the value of α. Here, we discuss the results for

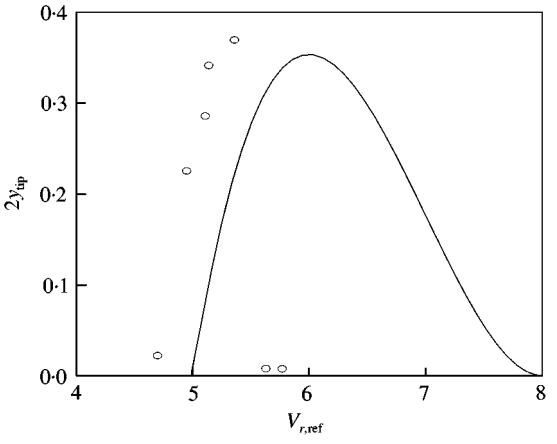

Figure 6. Predicted and measured responses for a uniform pivoted cylinder in a uniform flow. ○, measurements; ——, predicted response for all values of α.

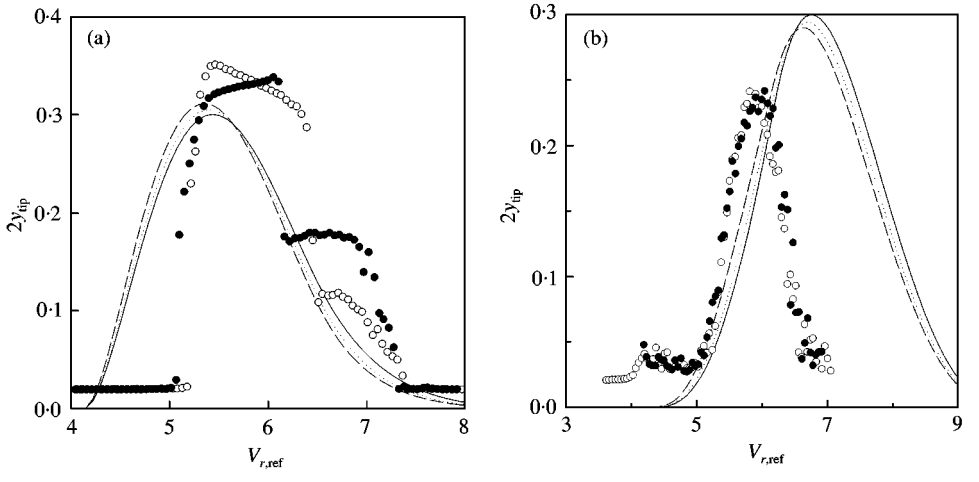

Figure 7. Predicted and measured responses for a uniform pivoted cylinder in linearly sheared flows. ○, measurements taken with $V_{r,\mathrm{ref}}$ increasing; ●, measurements taken with $V_{r,\mathrm{ref}}$ decreasing; full curves, predicted responses for various values of α: ——, $\alpha = 0$; ····, $\alpha = 1$; – – –, $\alpha = 1000$. (a) Minimum flow velocity at pivot; (b) maximum flow velocity at pivot.

$\alpha = 1$. For the flow velocity increasing along the length, the predicted maximum response is $2y_{\mathrm{tip}} = 0{\cdot}31$ at $V_{r,\mathrm{ref}} = 5{\cdot}44$ and the lock-in region ranges from $V_{r,\mathrm{ref}} = 4{\cdot}3$ to $8{\cdot}0$. The measured values are $2y_{\mathrm{tip}} = 0{\cdot}35$ at $V_{r,\mathrm{ref}} = 5{\cdot}47$ with lock-in ranging from $V_{r,\mathrm{ref}} = 5{\cdot}0$ to $7{\cdot}4$. The predicted maximum response is 11% less than the measured one. Again, the principle variance between the predicted and measured responses is in the extent of the lock-in region with the predicted lock-in region being wider than the measured one. For the flow velocity decreasing along the length, the predicted maximum response is $2y_{\mathrm{tip}} = 0{\cdot}29$ at $V_{r,\mathrm{ref}} = 6{\cdot}7$ and the lock-in region ranges from $V_{r,\mathrm{ref}} = 5{\cdot}0$ to $9{\cdot}0$. The measured values are $2y_{\mathrm{tip}} = 0{\cdot}24$ at $V_{r,\mathrm{ref}} = 5{\cdot}8$ with lock-in ranging from $V_{r,\mathrm{ref}} = 5{\cdot}0$ to $7{\cdot}0$. The predicted maximum is 20% higher than the measured one and its location is 16% higher. The major variance is again in the width of the lock-in region.

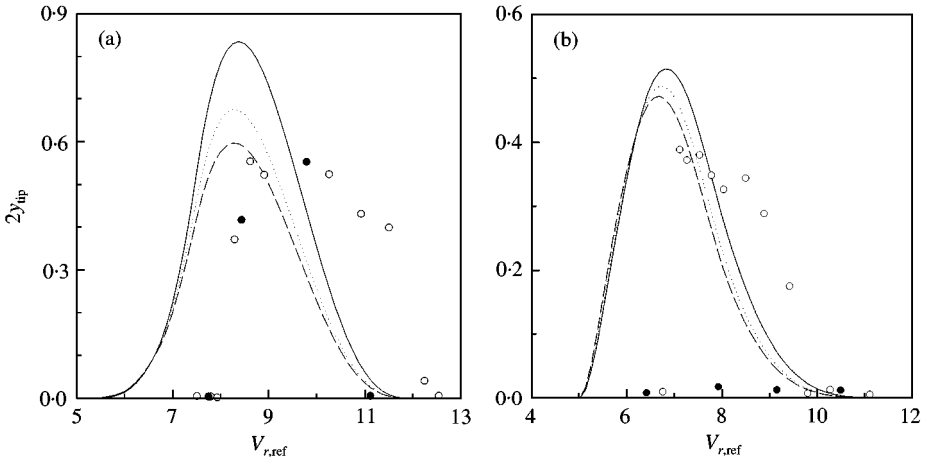

Figure 8. Predicted and measured responses for a tapered pivoted cylinder in a uniform flow. ○, measurements taken with $V_{r,\mathrm{ref}}$ increasing; ●, measurements taken with $V_{r,\mathrm{ref}}$ decreasing; full curves, predicted responses for various values of α: ——, $\alpha = 0$; ····, $\alpha = 1$; – – –, $\alpha = 1000$. (a) Pivot at small diameter end; (b) pivot at large diameter end.

5.2. Tapered Cylinders in Uniform Flows

The tapered cylinder had a length $L = 0{\cdot}603$ m, a maximum diameter $D_{\max} = 0{\cdot}05715$ m and a minimum diameter, also used as the reference diameter, $D_{\min} = D_{\mathrm{ref}} = 0{\cdot}0381$ m. The natural frequency when the small diameter end was pivoted was $f_n = 21$ Hz. For the large diameter end pivoted, the natural frequency was $f_n = 22$ Hz. For both situations, the damping ratio was $\xi = 0{\cdot}0022$.

The predicted and measured responses for the uniform flow case are shown in Figure 8. Figure 8(a) corresponds to the cylinder being pivoted at the small diameter end, Figure 8(b) to the pivot being at the large diameter end. The predicted response is shown for values of the stall parameter $\alpha = 0$, 1 and 1000. We note that, for the case represented in Figure 8(a), the predicted response becomes sensitive to the value of α. We again discuss the results for $\alpha = 1$. For the cylinder pivoted at its small diameter end, the predicted maximum response is $2y_{\mathrm{tip}} = 0{\cdot}68$ at $V_{r,\mathrm{ref}} = 8{\cdot}3$ and the lock-in region ranges from $V_{r,\mathrm{ref}} = 6{\cdot}0$ to $11{\cdot}0$. For the cylinder pivoted at its large diameter end, the predicted maximum response is $2y_{\mathrm{tip}} = 0{\cdot}49$ at $V_{r,\mathrm{ref}} = 6{\cdot}7$ and the lock-in region ranges from $V_{r,\mathrm{ref}} = 5{\cdot}0$ to 10.0. Both predicted maximum responses are about 25% larger than the measured ones. The locations of the predicted maximum responses are approximately 6% lower than the measured ones. In each instance, the predicted width of the lock-in region is somewhat greater than the measured width.

5.3. Tapered Cylinders in Linearly Sheared Flows

The results obtained by Balasubramanian *et al.* (2001) for the response of tapered cylinders in linearly sheared flows are not as reliable as the results discussed in Sections 5.1 and 5.2. They remark that the damping displayed some nonlinear characteristics and that it was difficult to select an appropriate value for the damping. They attribute this changed behavior to a possible deterioration of the air bearing at the cylinder pivot.

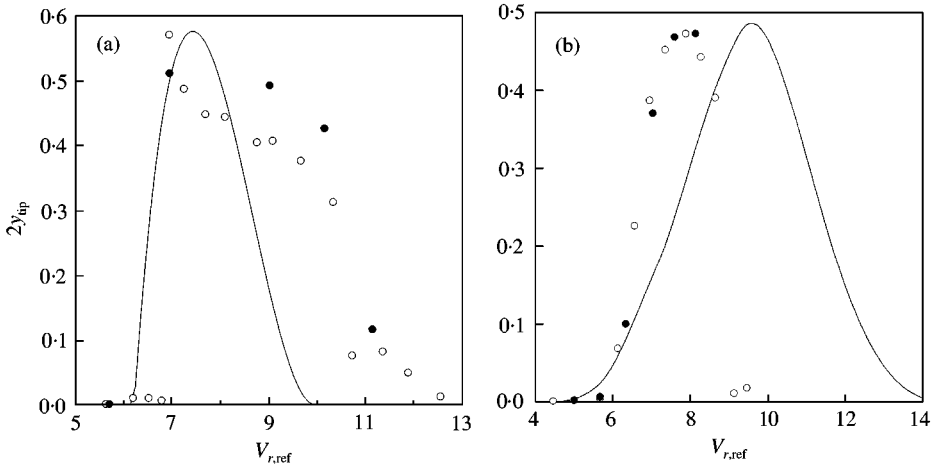

Figure 9. Predicted and measured responses for a tapered pivoted cylinder, with its small end pivoted, in linearly sheared flows. ○, measurements taken with $V_{r,ref}$ increasing; ●, measurements taken with $V_{r,ref}$ decreasing; ——, predicted responses for $\alpha = 1$. (a) Minimum flow velocity at pivot, $\xi = 0{\cdot}0027$; (b) maximum flow velocity at pivot, $\xi = 0{\cdot}0021$.

Hence, to compare the predictions of the inverse-direct method with the measured responses, we take a different approach. Namely, we vary the value of the damping ξ so that the predicted maximum response is identical with the measured maximum response and compare the other characteristics of the response. All calculations are done with the stall parameter α set to $\alpha = 1$.

The predicted and measured responses when the cylinder is pivoted at its small diameter end are shown in Figure 9. Figure 9(a) corresponds to the flow velocity increasing along the length of the cylinder, Figure 9(b) corresponds to the flow velocity decreasing along the length. The value of ξ used to generate Figure 9(a) is 0·0027, while that used to generate Figure 9(b) is 0.0021. For the flow velocity increasing along the length of the cylinder, the predicted maximum response is at $V_{r,ref} = 7{\cdot}5$ which is 9% higher than the measured location. The predicted lock-in region is narrower than the measured one. For the flow velocity decreasing along the length of the cylinder, the predicted maximum response is at $V_{r,ref} = 9{\cdot}5$ which is 20% higher than the measured location. The predicted lock-in region is now substantially wider than the measured one.

The predicted and measured responses when the cylinder is pivoted at its large diameter end are shown in Figure 10. Figure 10(a) corresponds to the flow velocity increasing along the length of cylinder, Figure 10(b) corresponds to the flow velocity decreasing along the length. The value of ξ used to generate Figure 10(a) is 0·0023, while that used to generate Figure 10(b) is 0·0027. For the flow velocity increasing along the length of the cylinder, the predicted maximum response is at $V_{r,ref} = 5{\cdot}7$ which is 5% lower than the measured location. The predicted and measured lock-in regions are quite similar. For the flow velocity decreasing along the length of the cylinder, the predicted maximum response is at $V_{r,ref} = 7{\cdot}5$. The measurements show a significant cylinder response only at $V_{r,ref} = 5{\cdot}7$.

5.4. Discussion

The agreement between the predictions of the inverse-direct method and the experimental data of Balasubramanian *et al.* (2000, 2001) for vortex-induced vibrations of uniform and

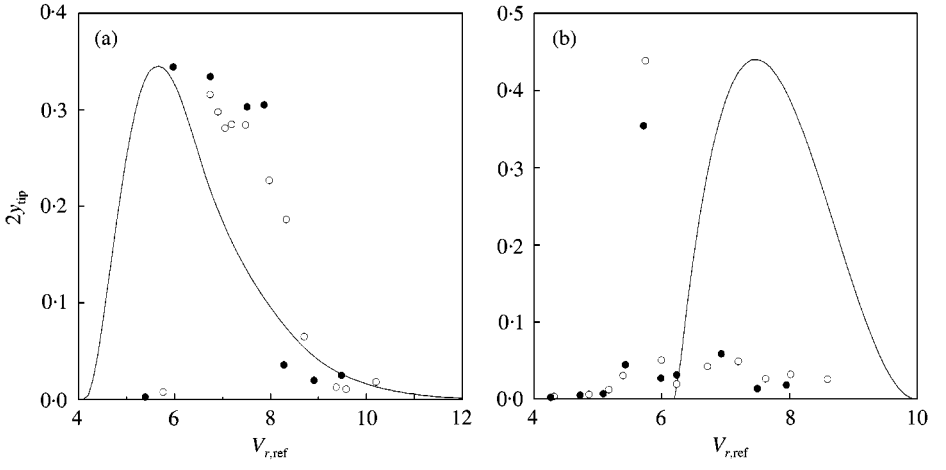

Figure 10. Predicted and measured responses for a tapered pivoted cylinder, with its large end pivoted, in linearly sheared flows. ○, measurements taken with $V_{r,\mathrm{ref}}$ increasing; ●, measurements taken with $V_{r,\mathrm{ref}}$ decreasing; ——, predicted responses for $\alpha = 1$. (a) Minimum flow velocity at pivot, $\xi = 0{\cdot}0023$; (b) maximum flow velocity at pivot, $\xi = 0{\cdot}0027$.

tapered pivoted cylinders in uniform and linearly sheared flows is quite good. The predicted peak vibration amplitudes range from -11% to $+25\%$ of the measured ones. This error is well within the bounds of previous results established for uniform cylinders in uniform flows. Referring to Figure 2, the values of $2A_{\max}$ for a given S_G frequently deviate by $\pm 100\%$ or more from the least-squares fit to the data. The predicted flow velocities at which the peak amplitudes occur are within -6% to $+20\%$ of the measured flow velocities. This error is also within the bounds of previous results for uniform cylinders in uniform flows. Referring to the appendix in Skop & Balasubramanian (1997), the values of V_{rp} in air range from 5·25 to 6·60 with a mean of 6·0. The spread about the mean is then 22%. The main discrepancy between the predictions and the measured data is in the extent of the lock-in regions, the predicted extents tending to be somewhat wider than the measured ones. However, we have already remarked that, for the uniform cylinder in uniform flow, the measured lock-in region is somewhat narrower than is usually observed.

5.5. Influence of k

The predicted responses of the uniform pivoted cylinder for $k = 4$ and values of the stall parameter $\alpha = 0$ and 1000 are shown in Figure 11, also shown is the baseline response for $k = 2$ and $\alpha = 1$. The responses shown are for linearly sheared flows. Figure 11(a) corresponds to the flow velocity increasing along the length of the cylinder, Figure 11(b) to the flow velocity decreasing along the length. We note that the baseline case is bounded by the $k = 4$ cases for both flow conditions. The same situation holds for other values of k and for flows over tapered cylinders. Hence, for any value of k, we can always find a value of α that will give nearly identical results to the $k = 2$ results. Thus, the use of $k = 2$ is justified.

6. CONCLUSIONS

A new method, the inverse-direct method, has been developed for predicting the vortex-induced vibrations of uniform and nonuniform cylinders in uniform and nonuniform flows. In the inverse portion of the method, the fluid force per unit length acting on a uniform

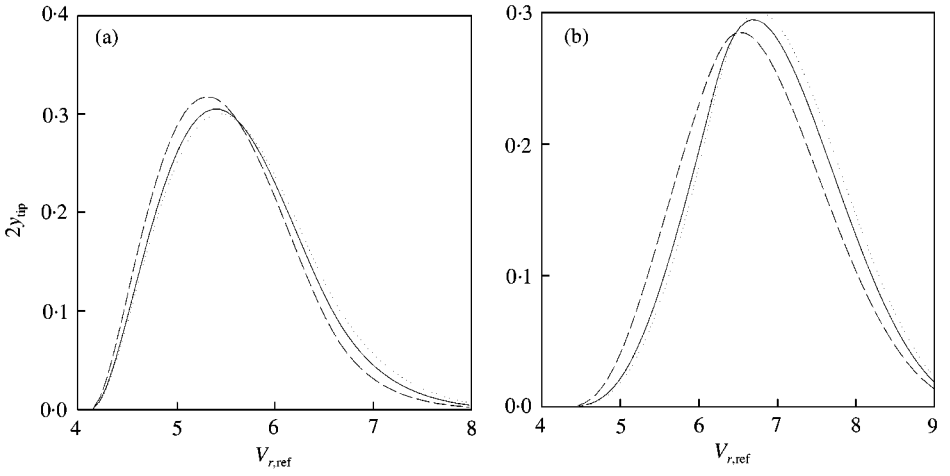

Figure 11. Influence of k on the predicted responses of a uniform pivoted cylinder in linearly sheared flows. Results are shown for $k = 4$ with $\alpha = 0$ and 1000 and for the baseline case $k = 2$ with $\alpha = 1$. (a) Minimum flow velocity at pivot; (b) maximum flow velocity at pivot: ——, $k = 2$, $\alpha = 1$; · · · · ·, $k = 4$, $\alpha = 0$; – – –, $k = 4$, $\alpha = 1000$.

cylinder in a uniform flow is determined from known experimental results. In the direct portion of the method, this force is applied locally along the cylinder.

We have shown that the inverse-direct method provides an explanation of the modal coupling patterns found experimentally for taut cables and beams in uniform flows. The predictions of the method also compare favorably with experimental data for the vortex-induced vibrations of uniform and tapered pivoted cylinders in uniform and sheared flows. Improvements in the comparisons could probably be achieved by changing the parameters or shape of the shape function $H(V_{r,i})$. However, this is not merited at present because of the scatter in the data for uniform flows over uniform cylinders and because of the fact that the experiments of Balasubramanian *et al.* (2000, 2001) were the first of their kind.

Overall, the inverse-direct method is easier to apply and yields more accurate predictions than the previously used nonlinear oscillator models.

ACKNOWLEDGEMENTS

The work reported here has been sponsored by the U.S. Office of Naval Research under Grants N00014-93-1-0438 (RAS) and N00014-96-1-0697 (GL, Dr Pratap Vanka PI), both monitored by Dr Tom Swean. The authors gratefully acknowledge this support. The authors would also like to thank Dr Charles Williamson for providing certain data files used in Khalak & Williamson (1999) and Dr Sathish Balasubramanian for providing several data files used in Balasubramanian *et al.* (2000, 2001).

REFERENCES

BALASUBRAMANIAN, S., HAAN JR, F. L., SZEWCZYK, A. A. & SKOP, R. A. 2001 An experimental investigation of the vortex-excited vibrations of axially varying pivoted cylinders in uniform and shear flow. *Journal of Wind Engineering and Industrial Aerodynamics* (in press).

BALASUBRAMANIAN, S., SKOP, R. A., HAAN JR, F. L. & SZEWCZYK, A. A. 2000 Vortex-excited vibrations of uniform pivoted cylinders in uniform and shear flow. *Journal of Fluids and Structures* **14,** 65–85.

BILLAH, K. Y. R. 1989 A study of vortex-induced vibrations. Ph.D. dissertation, Princeton University, Princeton, NJ, U.S.A.

BOKAIAN, A. 1994 Lock-in prediction of marine risers and tethers. *Journal of Sound and Vibration* **175,** 607–623.

GHARIB, M. R. 1999 Vortex-induced vibration, absence of lock-in and fluid force deduction. Ph.D. thesis, California Institute of Technology, Pasadena, CA, U.S.A.

GRIFFIN, O. M., PATTISON, J. H., SKOP, R. A., RAMBERG, S. E. & MEGGITT, D. J. 1980 Vortex-excited vibrations of marine cables. *ASCE Journal of the Waterway, Port, Coastal and Ocean Division* **106,** 183–204.

HARTLEN, R. & CURRIE, I. 1970 Lift-oscillator model for vortex-induced vibrations. *ASCE Journal of Engineering Mechanics* **96,** 577–591.

IWAN, W. D. 1975 The vortex induced oscillation of elastic structural elements. *ASME Journal of Engineering for Industry* **97,** 1378–1382.

IWAN, W. D. & BLEVINS, R. D. 1974 A model for vortex induced oscillation of structures. *Journal of Applied Mechanics* **41,** 581–586.

KHALAK, A. & WILLIAMSON, C. H. K. 1999 Motions, forces and mode transitions in vortex-induced vibrations at low mass-damping. *Journal of Fluids and Structures* **13,** 813–851.

PARKINSON, G. 1989 Phenomena and modelling of flow-induced vibrations of bluff bodies. *Progress in Aerospace Science* **26,** 169–224.

SARPKAYA, T. & ISAACSON, M. 1981 *Mechanics of Wave Forces on Offshore Structures.* New York: Van Nostrand Reinhold.

SKOP, R. A. & BALASUBRAMANIAN, S. 1997 A new twist on an old model for vortex-excited vibrations. *Journal of Fluids and Structures* **11,** 395–412.

SKOP, R. A. & GRIFFIN, O. M. 1973 A model for the vortex-excited response of bluff cylinders. *Journal of Sound and Vibration* **27,** 225–233.

SKOP, R. A. & GRIFFIN, O. M. 1975 On a theory for the vortex-excited oscillations of flexible cylindrical structures. *Journal of Sound and Vibration* **41,** 263–274.

THOMSON, W. T. 1965 *Vibration Theory and Applications.* Englewood Cliffs, NJ: Prentice-Hall.

TRIANTAFYLLOU, M. S., GOPALKRISHNAN, R. & GROSENBAUGH, M. S. 1994 Vortex-induced vibrations in a sheared flow: a new predictive method. In *Hydroelasticity in Marine Technology* (eds Faltinsen *et al.*), pp. 31–37. Rotterdam: Balkema.